



An effective and robust underwater image enhancement method based on color correction and artificial multi-exposure fusion

Ye Tao^{1,2} · Lili Dong¹ · Luqiang Xu² · Guangtong Chen² · Wenhai Xu¹

Received: 27 August 2021 / Revised: 25 October 2022 / Accepted: 13 March 2023 /

Published online: 24 March 2023

© The Author(s), under exclusive licence to Springer Science+Business Media, LLC, part of Springer Nature 2023

Abstract

Underwater images/frames are always subjected to color distortion, contrast reduction and detail loss, which degrade the visual quality severely. Current dehazing methods could not improve the visual quality of underwater images/frames robustly and effectively, especially in removing the undesired color cast. To address the issue, this paper introduces an effective and robust underwater image enhancement method without any dedicated hardware or prior knowledge. First, an adaptive reduction operation on the two stronger color-channels of inputs is employed to avoid the red over-compensated deficiency appearing in color-balanced result. Second, three kinds of color-balanced images are generated from the operation, which combines color compensation algorithms and famous Gray-World assumption. Third, a novel algorithm based on two non-reference quantitative evaluation indicators is utilized to choose the optimal color-balancing version. Then, gamma adjustment operation is employed to generate artificial over-/under-exposure visions of color-balancing image. Last, ‘exposedness’ and ‘contrast’ are set as two weights, being blended into the famous multi-scale fusion framework to generate the enhanced result. Our experimental results demonstrate the superior performance of the proposed method in both subjective and objective evaluations. Besides, the proposed method is also suitable for dehazing regular fogged images and local feature points matching.

Keywords Underwater image enhancement · Color-balance · Adaptive reduction algorithm · Artificial multi-exposure fusion strategy · Multi-scale fusion framework

✉ Ye Tao
taoye@dlmu.edu.cn

¹ School of Information Science and Technology, Dalian Maritime University, Dalian 116026, China

² Center of Technology, Liaoning Port Group Co., Ltd., Dalian 116001, China

1 Introduction

Underwater world provides numerous attractions for human beings, such as varieties of marine creatures, amazing landscapes, mysterious shipwrecks, and many available resources. Scientists therefore begin researching different branches of scientific areas of underwater world, such as underwater artificial facility inspection [8], target detection [9], marine organisms discovery [43], and robot control [42]. Unfortunately, degradation in visual quality of images and videos captured directly from underwater, which seriously limits human-beings to exploring and understanding the underwater world, because of the light scattering and absorption process [16, 27]. The scattering phenomenon always causes the direction of light propagation to change, while the absorption phenomenon reduces the energy of light seriously which results in color distortion. As a result, underwater images always appear color bias, low contrast and detail loss in visual perception. Generally, objects can be hardly recognized in water depths of more than 10 m without artificial light or some dedicated equipment, also the color is distorted.

A lot of techniques have been developed to dehaze underwater images. A few researchers, for instance, proposed to use dedicated hardware [1] or polarization-based strategies [46] to dehaze underwater images/frames. Although there are excellent results obtained by these approaches, the extremely expensive hardware limited them being applied in practical application. Additionally, some scientists proposed to use multiple-images dehazing methods [26] to enhance underwater images. However, acquiring multiple versions of the same scene in underwater environments was quite difficult to be operated. Therefore, proposing an effective underwater single image dehazing approach has become an issue that need to be addressed urgently. Underwater single image dehazing approaches could be generally classified into three main classes: Image enhancement approaches, image restoration approaches, and deep learning-based techniques.

According to the famous underwater imaging model, the most representative restoration method could be the Dark Channel Prior (DCP) [17], which was initially dedicated designed for dehazing fogged images. DCP assumed that most local patches in fogged images always had at least one color-channel with considerable low intensities. Then, He et al. proposed to estimate the thickness of haze and recovering degraded images through the assumption combining with the haze imaging model [17]. Although DCP exactly dehaze fogged images on most occasions, it failed in dehazing underwater images accurately since it ignored the light absorption phenomenon in underwater medium. After DCP, numerous underwater restoration approaches were presented. Hung et al. [45] proposed an approach which applied a color-correction operation after the DCP process. Wen et al. [41] proposed an adjusted imaging model to be applied in restoring underwater images. Drews et al. [10] proposed the famous Underwater Dark Channel Prior (UDCP), which was based on the observation that green and blue lights were the information source of inputs. Li et al. [22] proposed a dehazing method in green and blue channels and a correction method in red channel, which were used to restore underwater images. In more recent times, Berman et al. [35] proposed to expand the haze-line model to address the issue of wavelength dependent attenuation. Besides, Song et al. [5] proposed a new underwater dark channel prior restoration method, which made a great improvement in enhancing contrast. Nevertheless, such methods were always based on the combination of an extra color correction operation and the reversion of formular of the underwater imaging model, which required prior knowledge also hardly removed color-distortion accurately.

Underwater image enhancement approaches are always implemented by transforming in spatial/frequency domain or applying fusion framework, to correct color-distortion, enhance contrast and maintain detail-information for underwater images. Li et al. [23] proposed a minimum information loss and histogram distribution prior enhancement approach, which could enhance contrast and remove color distortion of inputs, but easily introduced red artifact into enhanced results. Fu et al. [14] proposed a ‘two-step’ strategy to enhance underwater images, which corrected the color-cast and enhanced contrast of inputs. However, the ‘two-step’ approach easily caused results suffering noise and undesired color cast. Later, Ancuti et al. [4] proposed to derive the contrast-enhanced version and the color-corrected version both from original inputs. Then, they employed ‘Laplacian contrast’, ‘local contrast’, ‘saliency’ and ‘exposedness’ as four weights, being blended into multi-scale fusion process. Unfortunately, results enhanced by [4] also always suffered from ‘red artifacts’ problem. In order to overcome the limitation, Ancuti et al. [2] proposed a new fusion strategy later, which was developed on the blending of the sharpened version and the gamma-corrected version directly derived from a color-corrected and white-balancing version of original underwater image. Then they used ‘Laplacian’, ‘saliency’ and ‘saturation’ as three weights to complete the fusing strategy. The later strategy overcame the limitation of their previous algorithm in a degree, but the results appeared in an unrealistic greyish tone and less clear too. Marques et al. [31] proposed the L²UWE which created two new models to generate two processed versions of the input. Then they took the multi-scale fusion scheme to enhance underwater images. Although L²UWE performed well in maintaining detail-information, it introduced too much noise into enhanced results and could not remove color distortion in underwater images. Recently, Zhuang et al. [48] developed a Bayesian retinex algorithm to improve the visual quality of inputs. But it could not maintain detail information, especially for images captured with artificial illumination.

Considering the great achievements in various applications of deep learning-based techniques, scientists also began to adopt them to dehaze underwater single image. Iqbal et al. [19] proposed an Unsupervised Color-correction Method (UCM), which was based on the combination of color balance, contrast correction of RGB color space and contrast correction of HSI color space. But UCM easily introduced red artifacts into enhanced results. In more recently, Song et al. [36] proposed a rapid scene depth estimation model combining date-driven supervised linear regression to train the model coefficients. Li et al. [24] proposed a novel underwater convolutional neural network model. But both methods required prior highly training dataset. In addition, Islam et al. [21] developed a fast underwater image enhancement method based on the generative adversarial network. However, it performed not well in inputs with uneven illumination.

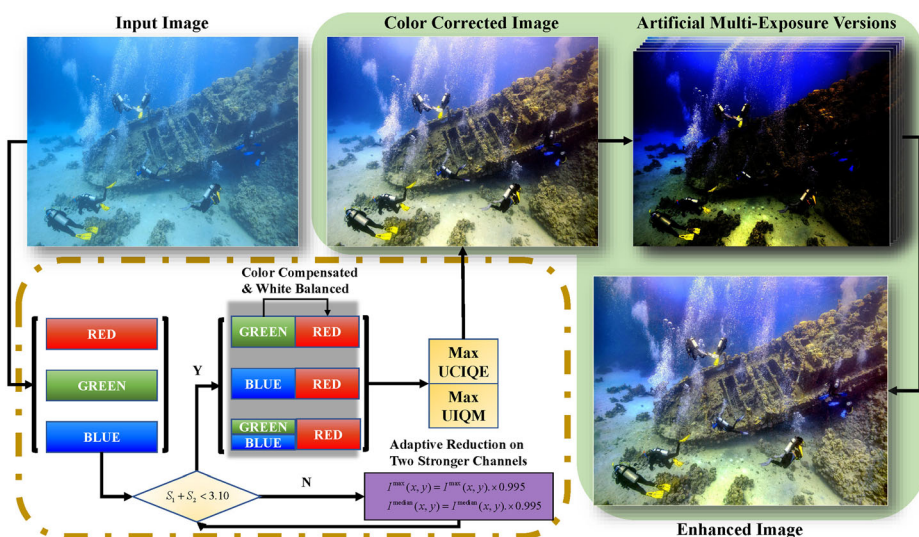
This paper introduces an effective underwater single image enhancement method, which employs a robust color correction method and an effective artificial multi-exposure fusion strategy. The technical contributions of this paper are summarized as follows:

- 1) A novel adaptive reduction algorithm on the two stronger color-channels of original image is creatively proposed, which effectively assists to generate a more accurate color corrected version from the input.
- 2) An effective color compensation algorithm is developed, which reasonably compensated degraded color of inputs.
- 3) A non-reference quantitative metric-based algorithm is presented to choose the optimal color-balanced version.

- 4) An effective artificial multi-exposure fusion strategy technique operation is utilized to enhance contrast and maintain details of color corrected results.
- 5) The proposed method effectively removes color cast, enhances contrast, and reconstructs details for underwater images. Besides, it can be also suitable for dehazing regular fogged images and improvement of local feature points matching task.

2 Method

Overview of our method is shown in Fig. 1, which contains two main steps: a Robust Color Correction (RCC) method and an effective artificial multi-exposure fusion strategy. In our RCC: First, a novel adaptive reduction algorithm is operated on the two stronger color-channels of the input, which comes from the observation of our analysis of 1000 randomly selected underwater images. Second, in view of the uncertainty of which color should be chosen to compensate the red channel. We propose three kinds of color compensation algorithms according to the classification of RUIE database [28], and utilize an effective color compensation algorithm which can be used to acquire three color-compensated versions from the input. Third, after the famous Gray-World assumption [47] operation on the three versions, a non-reference quantitative evaluation based algorithm is presented to choose the optimal color-balanced version, which comes from the sum-value of the Underwater Color Image Quality Evaluation (UCIQE) [44] and Underwater Image Quality Measure (UIQM) [33] metrics. In our effective artificial multi-exposure fusion strategy: We just utilize the gamma-adjustment operation to yield both over-/under-exposure versions of the color-balanced image without the Contrast Limited Adaptive Histogram Equalization (CLAHE) [34] operation on each of them. ‘Exposedness’ and ‘contrast’ weights are taken into the famous multi-scale fusion framework [7] to get the final enhanced result.



2.1 Robust color correction method

Traditional color correction methods refer to four white balancing approaches: The Gray-Edge assumption [37], the Shades-of-Gray assumption [11], the Max-RGB assumption [30] and the Gray-World assumption [6], which are designed for achieving the color constancy through dividing each channel by its corresponding normalized light source intensities [2]. However, only the Gray-World assumption [6] could yield a color-corrected version for underwater images, but easily caused ‘red artifact’ due to the very small mean-value of red channel in input. According to advantages and disadvantages of the existing mainstream of color-correction approaches, also combining the empirical results of our experiments with 1000 underwater images, we have summarized following four principles/hypothesis:

- (1) According to the wavelength dependent absorption phenomenon of light in underwater medium, and the advantage of Gray-World color balance in achieving color constancy for underwater images. Color channel compensation (3C) algorithm [2] should be utilized accordingly in correcting color distortion for underwater images. However, an adaptive reduction algorithm on the two stronger channels (with larger mean-value of pixel-intensity) of inputs should be employed before 3C, which could effectively assist to avoid ‘red artifacts’ appearing in corrected results, through our empirical results of experiments with 1000 underwater images.
- (2) Underwater images always appear greenish and bluish tones, but which one chosen to compensate red is an uncertain factor in current 3C algorithm. According to the classification of RUIE database [28], red color could be compensated from three situations probably: From blue channel, from green channel, and both from green and blue channels.
- (3) According to the disadvantage of 3C algorithm, it is easily neglected that green and blue channels should also be enhanced during the red compensation operation. We propose to use maximum-value and minimum value of green and blue channels to stretch intensities in corresponding channel as the operation introduced in [14], which assists to yield a more vivid color-corrected result.
- (4) UCIQE and UIQM which ranked 2nd and 3rd places in the comparison in terms of Pearson Linear Correlation Coefficient (PLCC) and Spearman Rankorder Correlation Coefficient (SROCC) [40], were specially designed for evaluating the quality of underwater color images. We decided to use these two metrics to choose the optimal version as our color-balanced result through a designed formulation.

2.1.1 Adaptive reduction algorithm

We analyze all 1000 images and their color-balanced results to find the relationship between the deviation and the appearance of deficiencies. It is necessary to introduce that 1000 images are selected randomly from the Underwater Image Enhancement Benchmark (UIEB) [25] dataset and UFO-120 database [20]. Interestingly, we observe that reducing the deviation between three channels of inputs through enhancing the weakest color-channel, which introduces more undesired artifact into results. We therefore

propose to reduce intensities of the strongest channel in original inputs. Meanwhile, for the sake of maintaining the basic tone of the inputs, the second strongest color-channel should also be reduced while the reduction being operated on the strongest one. However, reducing intensities of the two stronger color-channels could also lose the information of the original image. Therefore, finding the most suitable threshold value of the deviation between color-channels should be our next step. In order to demonstrate our analysis clearly, we first define some parameters as follows:

The deviation between the strongest and weakest channels as C_1 and the deviation between the second strongest and the weakest channel as C_2 ; We define some other parameters as follows:

$$S_1 = \frac{C_1}{\min[Rmean, Gmean, Bmean]} \quad (1)$$

$$S_2 = \frac{C_2}{\min[Rmean, Gmean, Bmean]} \quad (2)$$

Then comparing all parameters of 1000 images with related visual effect in balanced versions, and we find an interesting phenomenon. When the value of $S_1 + S_2$ is less than 3.10 in the input, the visual effect of its balanced version is always satisfied. So, we make a bold assumption that 3.10 is the threshold value of $S_1 + S_2$, which can assist to remove the color cast and not to introduce undesired artifacts effectively at the least cost of information loss. The algorithm of adaptive reduction on the two stronger color-channels of inputs can be represented as follows:

While ($S_1 + S_2 > 3.10$)

$$I_r^{\max}(x, y) = I^{\max}(x, y) \times 0.995 \quad (3)$$

$$I_r^{\text{median}}(x, y) = I^{\text{median}}(x, y) \times 0.995 \quad (4)$$

where $I^{\max}(x, y)$ and $I^{\text{median}}(x, y)$ signify pixel intensities in the strongest and the second strongest color-channels in each (x, y) . And $I_r^{\max}(x, y), I_r^{\text{median}}(x, y)$ denotes pixel intensities in the strongest and the second strongest channel after the adaptive reduction operation. 0.995 is an appropriate coefficient after numbers of tested to be used in the reduction operation. This approach could effectively avoid the undesired ‘red artifacts’ appearing at the least cost of information loss in final results. Figure 2 shows the effective improvement of the adaptive reduction algorithm.

2.1.2 Effective color compensation algorithm

First, the red channel compensated from green channel can be represented as follows:

$$I_c^R(x, y) = I^R(x, y) + \alpha \cdot (\bar{I}_G - \bar{I}_R) (1 - I^R(x, y)) \cdot I^G(x, y) \quad (5)$$

where $I_c^R(x, y)$ denotes the compensated red-channel, and $I^R(x, y), I^G(x, y)$ means the original red-/green-channel respectively. \bar{I}_G and \bar{I}_R signify the mean-values of original red- and green-

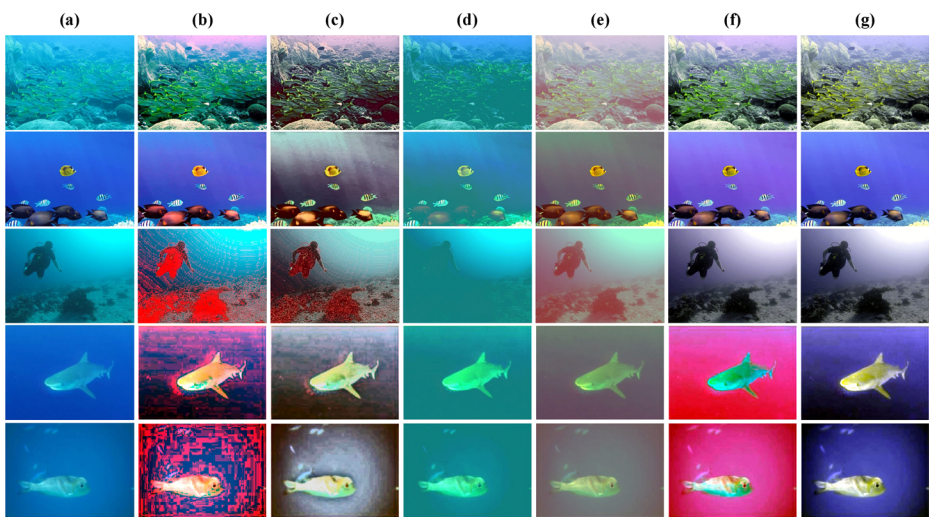


Fig. 2 Comparison of results from different color correction approaches (the value of $S1 + S2$ in each input is larger than 3.10). (a) Inputs. (b) Ancuti et al. [4]. (c) Fu et al. [12]. (d) Fu et al. [14]. (e) 3C. [2]. (f) Our robust color correction method (RCC) without the adaptive reduction operation. (g) Our RCC

channel. The parameter α can be set to 1 as the most appropriate value for most illumination conditions, which refers to [2]. And $I^R(x, y)$, $I^G(x, y)$, and $I^B(x, y)$ have been adjusted into the interval [0, 1] through a normalized procedure. In a similar way, we propose that the red channel compensated from blue channel can be represented as follows:

$$I_c^R(x, y) = I^R(x, y) + \alpha \cdot (\bar{I}_B - \bar{I}_R) (1 - I^R(x, y)) \cdot I^B(x, y) \quad (6)$$

And the red channel compensated from green and blue channels can be represented as follows:

$$\begin{aligned} I_c^R(x, y) &= I^R(x, y) + \frac{\alpha}{2} \cdot (\bar{I}_G - \bar{I}_R) (1 - I^R(x, y)) \cdot I^G(x, y) \\ &\quad + \frac{\alpha}{2} \cdot (\bar{I}_B - \bar{I}_R) (1 - I^R(x, y)) \cdot I^B(x, y) \end{aligned} \quad (7)$$

where \bar{I}_B signifies the mean-value pixel intensity of original blue channel. And the operation on green and blue channels can be represented as follows:

$$I_a^G(x, y) = \frac{I^G(x, y) - \min[I^G(x, y)]}{\max[I^G(x, y)] - \min[I^G(x, y)]} \quad (8)$$

$$I_a^B(x, y) = \frac{I^B(x, y) - \min[I^B(x, y)]}{\max[I^B(x, y)] - \min[I^B(x, y)]} \quad (9)$$

where $I_a^G(x, y)$, $I_a^B(x, y)$ means the adjusted green-/blue-channel respectively, and $\min[\cdot]$ and $\max[\cdot]$ denote the minimum-value and maximum-value of $[\cdot]$. Then we put three color-compensated images into the famous Gray-World assumption [6] and achieve three color-balanced versions of the input.

2.1.3 Optimal color balanced version selection algorithm

We propose the following equations to choose the optimal color-balanced version m , which is based on largest value of $\%IQA(m)$. The algorithm can be represented as follows:

$$\%UIQM = \left(\frac{UIQM(m) - \min[UIQM(m)]}{\max[UIQM(m)] - \min[UIQM(m)]} \right) \times 100 \quad (10)$$

$$\%UCIQE = \left(\frac{UCIQE(m) - \min[UCIQE(m)]}{\max[UCIQE(m)] - \min[UCIQE(m)]} \right) \times 100 \quad (11)$$

$$\%IQA(m) = \%UCIQE(m) + \%UIQM(m) \quad (12)$$

where $m \in [1, 2, 3]$ denotes three color-balanced version respectively. $UCIQE(m)$ and $UIQM(m)$ mean the scores in terms of UCIQE and UIQM that version m achieves

UCIQE [44]

The Underwater Color Image Quality Evaluation was proposed by Yang et al. in 2015, which was a linear combination of chroma, saturation and contrast. It was proposed to quantify the nonuniform color cast, blurring, and low contrast that characterize underwater engineering and monitoring images. The equation of UCIQE is represented as follows:

$$UCIQE = c_1 \times \sigma_c + c_2 \times con_l + c_3 \times \sigma_\mu \quad (13)$$

where σ_c , con_l , μ_s denotes the standard deviation of the chromaticity, the contrast and the mean-value of saturation respectively. c_1 , c_2 , and c_3 are set to 0.4680, 0.2745 and 0.2576 respectively, which are the three weighted coefficients. Higher value of UCIQE means better visual quality of evaluated image.

UIQM [33] The Underwater Image Quality Measure was proposed by Karen et al. in 2016, which comprised three underwater image attribute measures: the Underwater Image Colorfulness Measure (UICM), the Underwater Image Sharpness Measure (UISM), and the Underwater Image Contrast Measure (UIConM) to evaluate the underwater image quality. The equation of UIQM is represented as follows:

$$UIQM = c_1 \times UICM + c_2 \times UISM + c_3 \times UIConM \quad (14)$$

where c_1 , c_2 , and c_3 are three weighted coefficients set to 0.0282, 0.2953 and 3.5753 respectively. Higher value of UIQM also means better visual quality of evaluated image.

2.2 Effective artificial multi-exposure fusion strategy

Image contrast can be simply represented as follows:

$$C(\Omega) = I_{\max}^\Omega - I_{\min}^\Omega \quad (15)$$

where Ω signifies a given region from $I(x, y)$. $I_{\max}^\Omega \in [I(x, y)|(x, y) \in \Omega]$ and $I_{\min}^\Omega \in [I(x, y)|(x, y) \in \Omega]$. In general, I_{\max}^Ω denotes the darkest pixels in a given region of the image with accurate color

representation. On the contrary, I_{min}^{Ω} always denotes the brightest pixels in the same region. Therefore, recovering detail information, which can also assist to enhance contrast of the color-balanced image. In this work, we develop an artificial multiple exposure fusion strategy based on the famous multi-scale fusion framework [7]. Our fusion strategy is inspired by the AMEF [15], which utilizes the gamma-adjustment operation to yield five under-exposure versions artificially with different degrees and blends them into the multi-scale fusing scheme. Due to the deficiencies of AMEF that the utilized CLAHE [34] operation probably introduces too much artificial noise into result for underwater images. Meanwhile, considering that the saturation weight is able to change the corrected color information once again, observed in Fig. 3. We therefore propose to use the gamma-adjustment operation to yield different versions both in under-exposure and over-exposure of the color balanced image without the CLAHE operation. Then we just use the ‘exposedness’ and ‘contrast’ as two weights, blending into multi-scale fusing scheme to yield final-result. Figure 4 shows the flowchart of our effective artificial multiple exposure fusion strategy.

2.2.1 Input selection

Gamma adjustment operation is employed on the color corrected image to generate different exposure versions, which can be represented as follows:

$$I_{\gamma}(x, y) = I(x, y) \cdot ^{\wedge} \gamma \quad (16)$$

where γ is the positive constant, and $I_{\gamma}(x, y)$ denotes the adjusted exposure version of the $I(x, y)$. The value of γ influences the exposedness of output directly. We made some experiments to find the optimal values of γ , shown in Fig. 5. And the conclusions are summarized as follows:

- (1) The more versions with value of $\gamma < 1$ are taken into fusing process, the fusion result appears more fuzziness. And only one version with value of $\gamma = 0.5$ is appropriate for most situations to get a better fusion result.
- (2) The under-exposure versions with the value of $\gamma > 5$ almost hardly provide valuable information in their appearances.

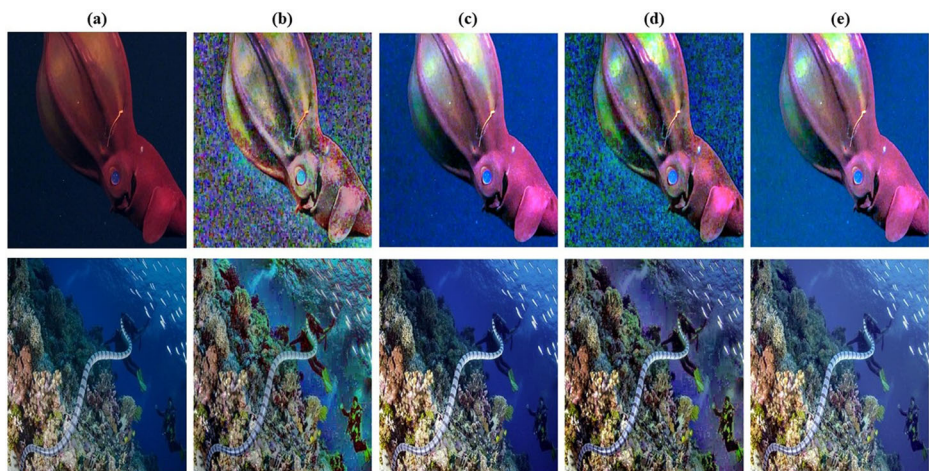


Fig. 3 Comparison of results from AMEF [15] and our fusion strategy. (a) Inputs. (b) AMEF on the inputs. (c) Our RCC. (d) AMEF on the color color corrected images. (e) Our fusion strategy on the color corrected images

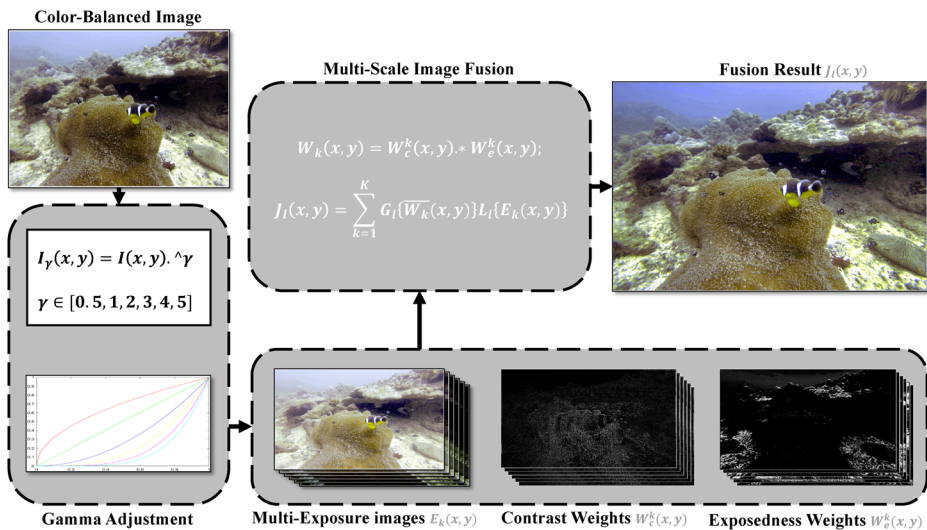


Fig. 4 Flowchart of our artificial multiple exposure fusion strategy

Therefore, we propose to define $\gamma = [0.5, 1, 2, 3, 4, 5]$ to generate six versions as $\{E_k = _1(x, y)| \gamma = 0.5, E_k = _2(x, y)| \gamma = 1, \dots, E_k = _6(x, y)| \gamma = 5\}$.

2.2.2 Weights definition

We therefore just set ‘contrast’ and ‘exposedness’ as two weights, blending into the fusion strategy, which can avoid change the original color-information of the color corrected version.

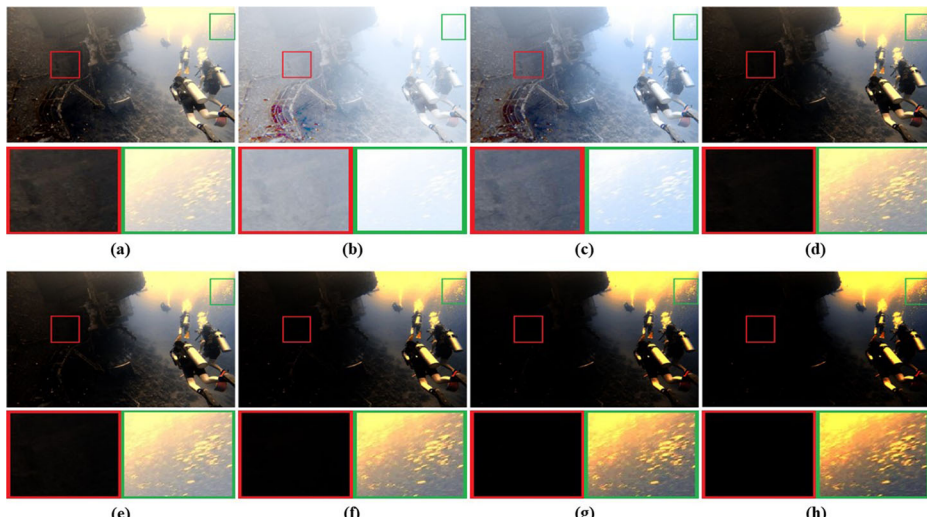


Fig. 5 Comparison of different values of γ . (a) Input. (b) $\gamma = 0.2$. (c) $\gamma = 0.5$. (d) $\gamma = 2$. (e) $\gamma = 3$. (f) $\gamma = 4$. (g) $\gamma = 5$. (h) $\gamma = 6$.

Contrast weight $W_c^k(x, y)$ According to [32], the contrast weight can be simply signified as the absolute value of the response to a simple Laplacian filter, formulated as:

$$W_c^k(x, y) = \frac{\partial^2 E_k}{\partial x^2}(x) + \frac{\partial^2 E_k}{\partial y^2}(y) \quad (17)$$

Exposedness weight $W_e^k(x, y)$ According to the [13], the exposedness weight can be defined as follows:

$$W_e^k(x, y) = \exp^{\frac{-0.5(E_k^c(x, y) - \beta)}{\sigma^2}} \quad (18)$$

where the standard deviation value σ and the illumination value β are set to 0.25 and 0.5 from the conclusion of [13]. And c denotes the R , G , B color-channel respectively.

Then the sum weight $W_k(x, y)$ is defined by simply combining multiplicatively $W_c^k(x, y)$ and $W_e^k(x, y)$ for each input $E_k(x, y)$ as follows:

$$W_k(x, y) = W_c^k(x, y) \times W_e^k(x, y) \quad (19)$$

In addition, a normalized operation is processed on $W_k(x, y)$, which aims for making sure intensities of the fusion result in range. The l^{th} level of fusion result $J_l(x, y)$ could be obtained as follows:

$$J_l(x, y) = \sum_{k=1}^K G_l \left\{ \overline{W}_k(x, y) \right\} L_l \{ E_k(x, y) \} \quad (20)$$

where $G_l\{\cdot\}$, $L_l\{\cdot\}$ means Gaussian/Laplacian pyramid decomposition transformation respectively, which is processed on the l^{th} level of normalized weights and inputs. The final fusion result $J(x, y)$ comes from reconstructing the Laplacian pyramid from bottom to top level. The proposed effective artificial multi-exposure fusion strategy can solve the contrast-degradation and detail-loss deficiencies for color corrected underwater images effectively.

3 Experiments and results

In this section, we first introduce the experiments settings. Secondly, we separately testify the performance of our RCC also the improvement of our whole strategy. Last, we introduce some extended applications of the proposed method.

3.1 Experiments settings

3.1.1 Testing images

To prove the effectiveness and robustness of our strategy, our comprehensive experiments are conducted on images from different datasets.

- 1) Underwater image enhancement benchmark (UIEB) [25]: A benchmark constructed of 850 underwater images with their corresponding non-degraded ones. We randomly choose 200 pairs of them to testify the improvement of our strategy.

- 2) Real-world underwater image enhancement dataset (RUIE) [28]: The database contains a total of 4230 underwater images, which are separated into 8 kinds of subset viz. green bias, green-blue bias, blue bias, also ‘A-E’ degree visual quality subsets according to degrees of their color deviation and visual quality. We randomly choose 100 images from each dataset (a total of 800 images) to testify the performance of our RCC.
- 3) Real-world underwater diving scenes dataset: We have captured 500 underwater diving images ourselves in the Bohai sea. We randomly choose 200 images to further verify the practical effect of our strategy.
- 4) Non-homogeneous hazy and haze-free image dataset (NH-HAZE) [3]: NH-HAZE provides 55 fogged images, also providing their corresponding ground-truth ones. We just randomly select 5 image-pairs to illustrate the extend application of our strategy.

3.1.2 Comparative methods

We choose Ancuti et al. [4], Fu et al. [12], Fu et al. [14], 3C [2] to compare the effect of color correction against our RCC. Besides, we also choose two underwater image enhancement methods: Marques et al. [31] and Zhuang et al. [48], two underwater image restoration methods: Song et al. [35] and Berman et al. [5], while another two deep learning-based solutions: Li et al. [24] and Islam et al. [21], to testify the improvement of our strategy. In order to obtain relevant dehazed results reliably, all comparative methods are operated through codes provided by their authors publicly released.

3.1.3 Evaluation metrics

Considering UCIQE [44] and UIQM [33] have been utilized in our RCC, we intend to employ another non-reference metric: Contrast index, Colorfulness index and Foggy index (CCF) [39] to evaluate the color corrected results obtained from different methods. CCF could evaluate underwater images based on quantification of the degrees of colorfulness, contrast and fog-density. Higher value of CCF means better visual quality of evaluated image too. In our underwater image dehazing comparison experiments, we exploit non-reference metrics: UCIQE [44], UIQM [33] also employ full-reference metrics: Structural Similarity Index Measurement (SSIM) [38] and Peak signal-to-noise ratio (PSNR) [18] to evaluate the underwater image dehazing effect. Thereinto, SSIM signifies a combination of luminance, contrast, and structure comparison between two image, higher value of SSIM means less differences between two images. While PSNR indicates the energy ratio of signal and noise, higher PSNR means that evaluated image with less extra noise.

3.1.4 Other technologies

To prove our strategy effectively improve the effect of local feature points matching, we employ a scale invariant feature transform (SIFT) [29] operator to compare the valid key-point matching number from images processed by different methods. Besides, we also exploit timing tools embedded in the MATLAB and Python to compare the computational efficiency of different methods.

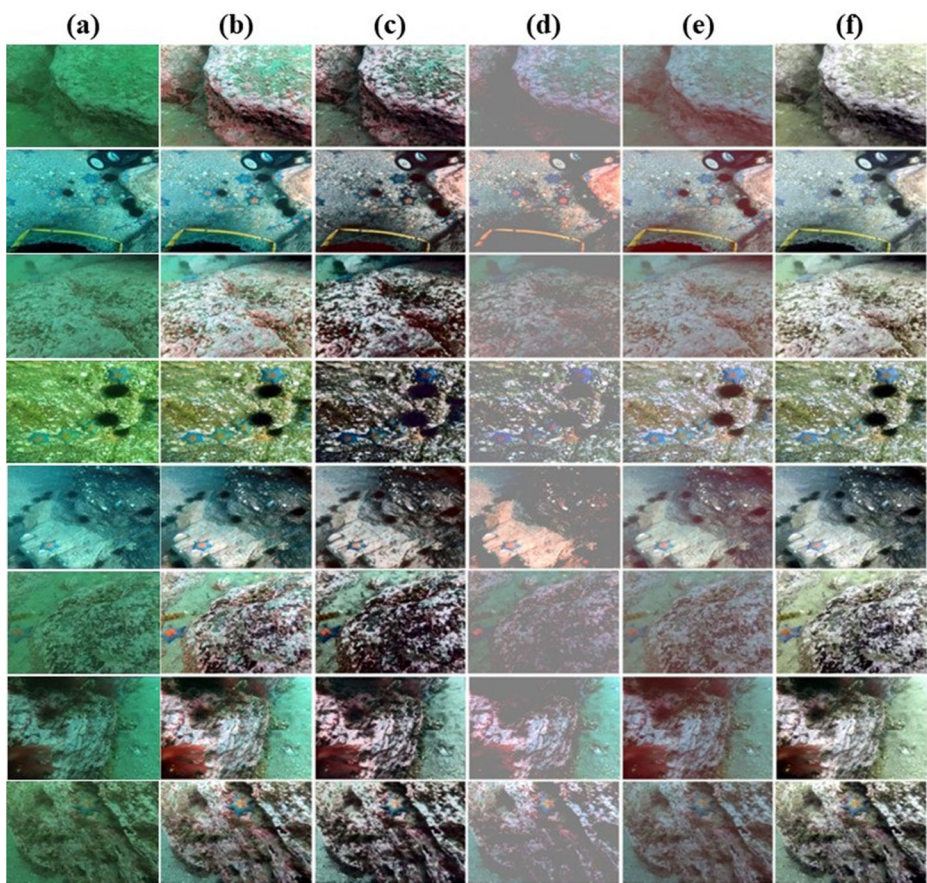


Fig. 6 Comparison of color corrected results. (a) Inputs. (b) Ancuti et al. [4]. (c) Fu et al. [12]. (d) Fu et al. [14]. (e) 3C [2]. (f) RCC. And row 1 to 8 are images with different classified degrees in RUIE database [28]: Row 1. ‘Green’ color cast. Row 2. ‘Blue’ color cast. Row 3. ‘Blue-Green’ color cast. Row 4. ‘A’ visual quality. Row 5. ‘B’ visual quality. Row 6. ‘C’ visual quality. Row 7. ‘D’ visual quality. Row 8. ‘E’ visual quality (the worst)

3.1.5 Experiments environments

We implement all experiments using MATLAB R2020b or Python 3.6 on a desktop with an Intel (R) Core (TM) I7-10700KF CPU @ 3.80 GHz processor.

3.2 RCC evaluation

Since color correction methods are proposed to remove the undesired color cast, the visual perception of color-corrected images is supposed to be the most important indicator in

Table 1 Comparison of average CCF on 800 images. Best scores are marked in bold

Methods	Ancuti et al. [4]	Fu et al. [12]	Fu et al. [14]	3C [2]	RCC
CCF	17.341	15.753	9.942	12.308	22.713

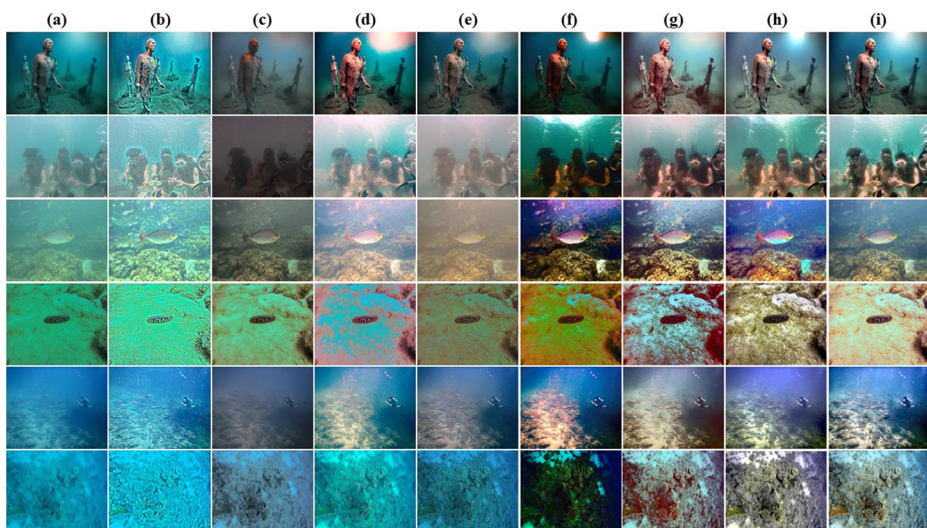


Fig. 7 Comparison of the dehazed results obtained from comparative techniques. **(a)** Input. **(b)** Marques et al. **(c)** Li et al. **(d)** Song et al. **(e)** Islam et al. **(f)** Berman et al. **(g)** Zhuang et al. **(h)** Ours. **(i)** Groundtruth images from UIEB

qualitative evaluations. Considering the RUIE database [28] has classified underwater images into different levels of color-casts and visual quality, we therefore employed images from the RUIE database [28] to compare the effect from our RCC and some state-of-the-art color correction methods (Ancuti et al. [4], Fu et al. [12], Fu et al. [14], 3C [2]). As can be observed in Fig. 6, color corrected versions obtained from Ancuti et al. [4] still suffer from color distortion. Fu et al. [12] makes the color-corrected results performing in an unrealistic dark appearance. Results obtained from Fu et al. [14] and 3C [2] have a similar ‘greyish’ background tone, which degrades contrast seriously. Besides, results obtained from the comparable color correction methods still exist ‘red artifacts’ more or less, due to the over-

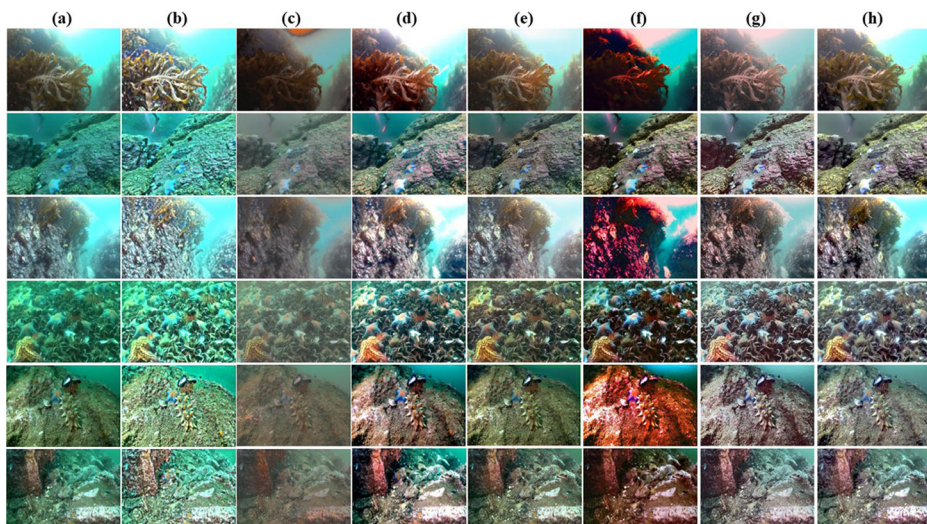


Fig. 8 Comparison of the dehazed results obtained from comparative techniques. **(a)** Input. **(b)** Marques et al. **(c)** Li et al. **(d)** Song et al. **(e)** Islam et al. **(f)** Berman et al. **(g)** Zhuang et al. **(h)** Ours

compensation operation on the red channel. Results obtained from our RCC appear more accurate color-correcting performance, and more vivid in visual perception.

Then we take 800 images (each 100 images comes from different classes of color-cast classifications and quality degradation degrees) from RUIE database into the quantitative evaluation based on the CCF, the average results of 800 images corrected by competitive methods are shown in Table 1. Our RCC achieves the highest score in terms of CCF compared with other methods, which further verifies the robustness and effectiveness of our RCC.

3.3 Proposed method evaluation

In this part, we adopt some images/frames from the UIEB database [25] and real-world underwater diving scenes dataset, to compare the dehazing performance with some state-of-the-art underwater dehazing approaches (Marques et al. [31], Li et al. [24], Song et al. [35], Islam et al. [21], Berman et al. [5], and Zhuang et al. [48]).

3.3.1 Qualitative comparison

The comparison of results for some random examples from UIEB database [25] and our diving dataset are shown in Fig. 7 and Fig. 8.

Table 2 Comparison of the SSIM, PSNR, UCIQE, and UIQM of Fig. 7. Best scores are marked in bold

Image	Metrics	Marques et al. [31]	Li et al. [24]	Song et al. [35]	Islam et al. [21]	Berman et al. [5]	Zhuang et al. [48]	Ours
Image 1	SSIM	0.612	0.719	0.729	0.727	0.709	0.844	0.920
	PSNR	14.474	17.672	20.064	16.930	14.835	16.672	18.344
	UCIQE	0.577	0.459	0.678	0.579	0.609	0.599	0.629
	UIQM	2.253	2.219	1.994	2.646	1.484	2.416	2.258
Image 2	SSIM	0.624	0.166	0.578	0.579	0.601	0.625	0.928
	PSNR	13.972	9.629	15.227	15.520	11.250	19.789	21.070
	UCIQE	0.457	0.389	0.508	0.396	0.628	0.579	0.635
	UIQM	3.215	1.565	2.629	2.332	1.984	3.082	3.102
Image 3	SSIM	0.680	0.544	0.718	0.720	0.518	0.871	0.872
	PSNR	14.919	17.312	13.795	14.990	13.105	17.570	16.177
	UCIQE	0.445	0.447	0.464	0.378	0.359	0.640	0.698
	UIQM	3.131	2.527	2.804	2.607	2.356	2.471	2.146
Image 4	SSIM	0.084	0.552	0.718	0.772	0.504	0.539	0.801
	PSNR	10.372	12.827	13.795	17.779	8.549	16.798	19.081
	UCIQE	0.492	0.447	0.589	0.447	0.578	0.607	0.650
	UIQM	2.593	2.527	2.930	3.187	1.927	2.842	2.792
Image 5	SSIM	0.646	0.601	0.772	0.771	0.764	0.898	0.899
	PSNR	14.862	12.961	19.287	17.779	17.241	18.048	19.237
	UCIQE	0.480	0.428	0.569	0.507	0.606	0.582	0.611
	UIQM	2.163	2.262	2.394	2.898	2.224	2.686	2.877
Image 6	SSIM	0.313	0.620	0.385	0.323	0.281	0.690	0.870
	PSNR	9.784	17.338	11.652	10.794	7.827	13.473	18.341
	UCIQE	0.444	0.427	0.451	0.430	0.595	0.577	0.618
	UIQM	1.762	2.262	1.847	2.597	1.573	2.812	3.178
Mean-value of 200 images	SSIM	0.487	0.531	0.666	0.601	0.579	0.783	0.806
	PSNR	13.241	14.094	15.131	15.674	12.363	17.591	17.991
	UCIQE	0.490	0.447	0.550	0.448	0.588	0.602	0.627
	UIQM	2.499	2.315	2.428	2.801	2.004	2.743	2.811

Table 3 Comparison of the UCIQE and UIQM of Fig. 8. Best scores are marked in bold

Image	Metrics	Marques et al. [31]	Li et al. [24]	Song et al. [35]	Islam et al. [21]	Berman et al. [5]	Zhuang et al. [48]	Ours
Image 1	UCIQE	0.628	0.541	0.649	0.602	0.629	0.564	0.652
	UIQM	2.850	1.982	2.169	2.879	1.626	1.801	2.855
Image 2	UCIQE	0.532	0.444	0.604	0.517	0.613	0.581	0.631
	UIQM	2.144	2.987	2.605	3.266	2.447	3.087	2.874
Image 3	UCIQE	0.544	0.479	0.589	0.519	0.601	0.577	0.636
	UIQM	2.928	2.696	3.002	3.284	1.752	2.744	3.496
Image 4	UCIQE	0.543	0.445	0.630	0.566	0.628	0.600	0.605
	UIQM	2.208	3.488	2.854	3.636	2.635	3.430	3.434
Image 5	UCIQE	0.605	0.427	0.625	0.599	0.631	0.587	0.613
	UIQM	1.928	3.104	2.066	3.081	1.702	3.095	3.569
Image 6	UCIQE	0.597	0.455	0.622	0.573	0.619	0.568	0.618
	UIQM	2.337	3.297	2.465	3.495	2.289	3.336	3.671
Mean-value of 200 images	UCIQE	0.536	0.474	0.591	0.507	0.601	0.575	0.613
	UIQM	2.526	2.654	2.582	3.001	2.254	2.711	3.076

As observed, Marques et al. [31] recovers lost details to a certain extent, but it introduces too much noise into enhanced result, which degrades visual quality a lot. Meanwhile, Marques et al. [31] also could not remove color distortion of underwater images both in Fig. 7 and Fig. 8. And also the enhancement method: Zhuang et al. [48], although it performs well in the comparison with our experimental images, it introduces undesired ‘red artifact’ into enhanced results especially in Fig. 7. The restoration methods: Song et al. [35] and Berman et al. [5], which appear unstable effect for dehazing underwater images. They may further darken the restored images sometimes, which cause details hardly being recognized in the final version. Also, they could not correct color bias accurately sometimes. The deep learning-based techniques: Li et al. [24] and Islam et al. [21], which hardly improve the visual quality of underwater images due to lack of enough prior training. The qualitative comparisons in Fig. 7 and Fig. 8 fully demonstrate the superiority of our method, which could not only remove color cast accurately, but also enhance contrast and reconstruct lost details effectively.

3.3.2 Quantitative comparison

In order to evaluate dehazed results obtained from comparative methods comprehensively, we therefore decide to employ non-reference quantitative evaluations metrics and full-reference ones to make a comparison. However, since images provided from our diving dataset do not have the ground-truth reference images, so we just utilize non-reference metrics to evaluate them in terms of UCIQE and UIQM. Corresponding quantitative results of Fig. 7 are shown in Table 2, and results of Fig. 8 are shown in Table 3. The higher score all employed evaluation metrics achieve, the better the visual quality of evaluated images are better.

Table 4 Comparison of computational efficiency of comparative techniques. Best scores are marked in bold

Methods	Marques et al. [31]	Li et al. [24]	Song et al. [35]	Islam et al. [21]	Berman et al. [5]	Zhuang et al. [48]	Ours
Runtime(s)	1.272	4.064	0.593	0.561	1.306	0.694	0.517



Fig. 9 Evaluation on regular fogged images from NH-HAZE database [3]. Row 1. Original images. Row 2. Ours. Row 3. Reference images

As can be observed in Table 2, our method almost achieves the top three scores in terms of UIQM and PSNR of all images, while in UCIQE and SSIM comparison, our method performs even better. Besides, our method achieves top scores in terms of all metrics for mean-value of randomly selected 200 images. Table 3 also proves the superiority of our method.

3.4 Computational efficiency comparison

Since Islam et al. [21] fixes the input to the size of 256×256 first. Therefore, we also employ this size to make the computational efficiency comparison, which is shown in Table 4. And our method takes about 0.517 (s), which ranks the 1st place in this comparison.

3.5 Extend applications

Although our method is dedicated designed for dehazing underwater images, it works well in dehazing regular hazy images too. Figure 9 shows the effect of our method processing on some fogged images from the NH-HAZE database. Table 5 shows the objective evaluation results of Fig. 9 in terms of PSNR and SSIM. Images enhanced by our method appear a significant

Table 5 Comparison of the PSNR and SSIM of Fig. 9. Best scores are marked in bold

Input			Ours	
	PSNR	SSIM	PSNR	SSIM
Image 1	13.6042	0.4940	15.2958	0.5130
Image 2	12.1118	0.4850	14.8157	0.5180
Image 3	11.7352	0.5031	14.3909	0.5504
Image 4	10.4520	0.3769	10.7594	0.4003
Image 5	10.2932	0.3146	11.5247	0.3200

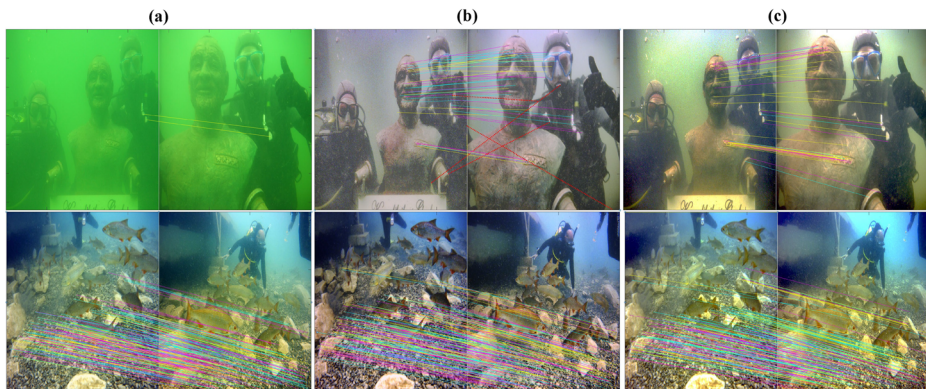


Fig. 10 Matched results based on SIFT [29] operator, and the mismatches are marked in red and bold. **(a)**. original images. **(b)**. 3C [2]. **(c)**. Ours

improvement in visual perception. The quantitative results also prove the effectiveness of our method on fogged images.

In addition, our method is also suitable for local feature points matching, which is an important task of vision computer applications. We utilize the Scale Invariant Feature Transform (SIFT) operator [29] to compute the number of matched key-points in original underwater image, enhanced by 3C [2] and enhanced by our method. Figure 10 and Table 6 show the comparison of the number of matched key-points in related images. Our method achieves more numbers of valid matched key-points both in the inputs with good or bad visual quality.

4 Conclusion

Current underwater image dehazing methods could not dehaze underwater images effectively and robustly, especially in removing undesired color bias. Therefore, this paper presents an effective and robust underwater image enhancement method. First, a robust color correction method is employed to generate a color balanced version of the input, which mainly contains an adaptive reduction algorithm, an adjusted compensation operation, a famous Gray-World assumption operation and a non-reference metric-based selection algorithm. Then an effective artificial multi-exposure fusion process is operated on the color corrected version to enhance contrast and reconstruct detail-information. The proposed method generally performs better than some previous underwater dehazing algorithms, through our experiments in terms of both objective and subjective evaluations, especially in removing color distortion. Besides, our method can also be used for local feature points matching tasks and dehazing fogged images.

Table 6 Comparison of numbers of matched key-points in Fig. 10. Best scores are marked in bold

Input	3C [2]		Ours	
	Misses	Valid matches	Misses	Valid matches
Image 1	0	2	4	40
Image 2	0	270	0	275

However, in our quantitative evaluating experiments, some enhanced images appeared with better visual perception but acquired lower scores in UCIQE and UIQM, which demonstrated that the UCIQE and UIQM also had their own limitations. Therefore, there was a possibility that the chosen version was not the optimal color-balanced version. We thus intend to continue our research for proposing a more suitable algorithm to choose the optimal result in our future work.

Acknowledgements The author(s) disclosed receipt of the following financial support for the research, authorship, and/or publication of this article: This paper is supported by National Key Research and Development Program of China under Grant 2019YFB1600400. This paper is also supported in part by the Fundamental Research Funds for the Central Universities of China under Grant 3132019340 and 3132019200, and high-tech ship research project from ministry of industry and information technology of the people's republic of China under Grant MC-201902-C01.

Data availability Datasets (UIEB, RUIE, and NH-HAZE) used for testing relevant underwater dehazing methods have been taken from following digital object identifiers: doi: <https://doi.org/10.1109/TIP.2019.2955241>, doi: <https://doi.org/10.1109/TCSVT.2019.2963772>, and doi: <https://doi.org/10.1109/CVPRW50498.2020.00230>. Diving scenes dataset used for testing relevant underwater image dehazing methods in this paper, is available from the corresponding author on reasonable request.

References

1. Alex Raj SM, Supriya MH (2016) Underwater image enhancement using single scale retinex on a reconfigurable hardware. International Symposium on Ocean Electronics, SYMPOL
2. Ancuti CO, Ancuti C, De Vleeschouwer C et al (2018) Color balance and fusion for underwater image enhancement. IEEE Trans Image Process 27(1):379–393
3. Ancuti CO, Ancuti C, Timofte R (2020) NH-HAZE: An image dehazing benchmark with non-homogeneous hazy and haze-free images. IEEE Computer Society Conference on Computer Vision and Pattern Recognition Workshops. pp. 1798–1805
4. Ancuti C, Ancuti CO, Haber T et al (n.d.) Enhancing underwater images and videos by fusion. Proceedings of the IEEE Computer Society Conference on Computer Vision and Pattern Recognition. pp. 81–88
5. Berman D, Levy D, Avidan S et al (2020) Underwater single image color restoration using haze-lines and a new quantitative dataset. IEEE transactions on pattern analysis and machine intelligence
6. Buchsbaum G (1980) Spatial processor model for object colour perception. J Franklin Institute 310(1):1–26
7. Burt PJ, Adelson EH (1983) LAPACIAN pyramid as a compact image code. IEEE Trans Commun COM-31(4):532–540
8. Chen W, Gu K, Lin W, Yuan F, Cheng E (2020) Statistical and structural information backed full-reference quality measure of compressed sonar images. IEEE Trans Circ Syst Vid Technol 30(2):334–348
9. Chen X, Yu J, Kong S, Wu Z, Wen L (2021) Joint anchor-feature refinement for real-time accurate object detection in images and videos. IEEE Trans Circ Syst Vid Technol 31(2):594–607
10. Drews-Jr P, Do Nascimento E, Moraes F et al. (n.d.) Transmission estimation in underwater single images. Proceedings of the IEEE International Conference on Computer Vision. pp. 825–830
11. Finlayson GD, Trezzi E (n.d.) Shades of gray and colour constancy. Final Program and Proceedings - IS and T/SID Color Imaging Conference. pp. 37–41
12. Fu X, Zhuang P, Huang Y et al. (2014) A retinex-based enhancing approach for single underwater image," 2014 IEEE international conference on image processing, ICIP. pp. 4572–4576.
13. Fu X, Zeng D, Huang Y, Liao Y, Ding X, Paisley J (2016) A fusion-based enhancing method for weakly illuminated images. Signal Process 129:82–96
14. Fu X, Fan Z, Ling M et al. (2018) Two-step approach for single underwater image enhancement," 2017 International Symposium on Intelligent Signal Processing and Communication Systems, ISPACS 2017 - Proceedings. pp. 789–794
15. Galdran A (2018) Image dehazing by artificial multiple-exposure image fusion. Signal Process 149:135–147
16. Hayat N, Imran M (2020) Detailed and enhanced multi-exposure image fusion using recursive filter. Multimed Tools Appl 79(33–34):25067–25088
17. He K, Sun J, Tang X (2011) Single image haze removal using dark channel prior. IEEE Trans Pattern Anal Mach Intell 33(12):2341–2353

18. Huynh-Thu Q, Ghanbari M (2008) Scope of validity of PSNR in image/video quality assessment. *Electron Lett* 44(13):800–801
19. Iqbal K, Odetayo M, James A et al. (n.d.) Enhancing the low quality images using unsupervised colour correction method. Conference Proceedings - IEEE International Conference on Systems, Man and Cybernetics. 1703-1709
20. Islam MJ, Luo PG, Sattar J (2020) [simultaneous enhancement and super-resolution of underwater imagery for improved visual perception] Mit press, Cambridge
21. Islam MJ, Xia Y, Sattar J (2020) Fast underwater image enhancement for improved visual perception. *IEEE Robot Automa Lett* 5(2):3227–3234
22. Li C, Quo J, Pang Y et al. (2016) Single underwater image restoration by blue-green channels dehazing and red channel correction. ICASSP, IEEE International Conference on Acoustics, Speech and Signal Processing - Proceedings. pp. 1731-1735
23. Li C-Y, Guo J-C, Cong R-M, Pang YW, Wang B (2016) Underwater image enhancement by Dehazing with minimum information loss and histogram distribution prior. *IEEE Trans Image Process* 25(12):5664–5677
24. Li C, Anwar S, Porikli F (2020) Underwater scene prior inspired deep underwater image and video enhancement. *Pattern Recogn* 98:107038
25. Li C, Guo C, Ren W, Cong R, Hou J, Kwong S, Tao D (2020) An underwater image enhancement benchmark dataset and beyond. *IEEE Trans Image Process* 29:4376–4389
26. Lin W-H, Zhong J-X, Liu S et al. (2020) ROIMIX: Proposal-Fusion among Multiple Images for Underwater Object Detection. ICASSP, IEEE International Conference on Acoustics, Speech and Signal Processing – Proceedings. pp. 2588–2592
27. Liu K, Li X (2021) De-hazing and enhancement method for underwater and low-light images, De-hazing and enhancement method for underwater and low-light images
28. Liu R, Fan X, Zhu M, Hou M, Luo Z (2020) Real-world underwater enhancement: challenges, benchmarks, and solutions under natural light. *IEEE Trans Circ Syst Vid Technol* 30(12):4861–4875
29. Lowe DG (2004) Distinctive image features from scale-invariant keypoints. *Int J Comput Vis* 60(2):91–110
30. Marini D, Rizzi A (n.d.) A computational approach to color illusions. Lecture Notes in Computer Science (including subseries Lecture Notes in Artificial Intelligence and Lecture Notes in Bioinformatics). 1310. pp. 62–69
31. Marques TP, Branzan Albu A (2020) L2UWE: A framework for the efficient enhancement of low-light underwater images using local contrast and multi-scale fusion. IEEE Computer Society Conference on Computer Vision and Pattern Recognition Workshops. pp. 2286–2295
32. Mertens T, Kautz J, Van Reeth F (n.d.) Exposure fusion. Proceedings - Pacific Conference on Computer Graphics and Applications. pp. 382–390
33. Panetta K, Gao C, Agaian S (2016) Human-visual-system-inspired underwater image quality measures. *IEEE J Ocean Eng* 41(3):541–551
34. Pizer SM, Johnston RE, Erickson JP et al. (n.d.) Contrast-limited adaptive histogram equalization: Speed and effectiveness. pp. 337–345
35. Song W, Wang Y, Huang D, Liotta A, Perra C (2020) Enhancement of underwater images with statistical model of background light and optimization of transmission map. *IEEE Trans Broadcast* 66(1):153–169
36. Song W, Wang Y, Huang D et al (n.d.) A rapid scene depth estimation model based on underwater light attenuation prior for underwater image restoration. Lecture Notes in Computer Science (including subseries Lecture Notes in Artificial Intelligence and Lecture Notes in Bioinformatics). 11164 LNCS. pp. 678–688
37. van de Weijer J, Gevers T, Gijsenij A (2007) Edge-based color constancy. *IEEE Trans Image Process* 16(9): 2207–2214
38. Wang Z, Bovik AC, Sheikh HR, Simoncelli EP (2004) Image quality assessment: from error visibility to structural similarity. *IEEE Trans Image Process* 13(4):600–612
39. Wang Y, Li N, Li Z, Gu Z, Zheng H, Zheng B, Sun M (2018) An imaging-inspired no-reference underwater color image quality assessment metric. *Comput Electr Eng* 70:904–913
40. Wang Y, Song W, Fortino G, Qi LZ, Zhang W, Liotta A (2019) An experimental-based review of image enhancement and image restoration methods for underwater imaging. *IEEE Access* 7:140233–140251
41. Wen H, Tian Y, Huang T et al (n.d.) Single underwater image enhancement with a new optical model. Proceedings - IEEE International Symposium on Circuits and Systems. pp. 753–756
42. Williams SB, Pizarro OR, Jakuba MV, Johnson CR, Barrett NS, Babcock RC, Kendrick GA, Steinberg PD, Heyward AJ, Doherty PJ, Mahon I, Johnson-Roberson M, Steinberg D, Friedman A (2012) Monitoring of benthic reference sites: using an autonomous underwater vehicle. *IEEE Robot Autom Mag* 19(1):73–84
43. Yan H, Wu Q, Yu C et al. (2020) Recent Progress of Biomimetic Antifouling Surfaces in Marine. *Adv Mat Inter*, 7(20)
44. Yang M, Sowmya A (2015) An underwater color image quality evaluation metric. *IEEE Trans Image Process* 24(12):6062–6071

45. Yang H-Y, Chen P-Y, Huang C-C et al. (2011) Low complexity underwater image enhancement based on dark channel prior. Proceedings - 2011 2nd international conference on innovations in bio-inspired computing and applications, IBICA. pp. 17–20
46. Yang K, Liu F, Han P et al (2019) Real-time active underwater polarization descattering. Optics InfoBase Conference Papers. Part F170-COSI
47. Zhang H, Dong B, Jiang Z (n.d.) Single Image Dehazing Using Improved Gray World Theory and Dark Channel Prior. Lecture Notes in Computer Science (including subseries Lecture Notes in Artificial Intelligence and Lecture Notes in Bioinformatics). 11717 LNCS. pp. 67–73
48. Zhuang P, Li C, Wu J (2021) Bayesian retinex underwater image enhancement. Eng Appl Artif Intell 101: 104171

Publisher's note Springer Nature remains neutral with regard to jurisdictional claims in published maps and institutional affiliations.

Springer Nature or its licensor (e.g. a society or other partner) holds exclusive rights to this article under a publishing agreement with the author(s) or other rightsholder(s); author self-archiving of the accepted manuscript version of this article is solely governed by the terms of such publishing agreement and applicable law.

Terms and Conditions

Springer Nature journal content, brought to you courtesy of Springer Nature Customer Service Center GmbH (“Springer Nature”).

Springer Nature supports a reasonable amount of sharing of research papers by authors, subscribers and authorised users (“Users”), for small-scale personal, non-commercial use provided that all copyright, trade and service marks and other proprietary notices are maintained. By accessing, sharing, receiving or otherwise using the Springer Nature journal content you agree to these terms of use (“Terms”). For these purposes, Springer Nature considers academic use (by researchers and students) to be non-commercial.

These Terms are supplementary and will apply in addition to any applicable website terms and conditions, a relevant site licence or a personal subscription. These Terms will prevail over any conflict or ambiguity with regards to the relevant terms, a site licence or a personal subscription (to the extent of the conflict or ambiguity only). For Creative Commons-licensed articles, the terms of the Creative Commons license used will apply.

We collect and use personal data to provide access to the Springer Nature journal content. We may also use these personal data internally within ResearchGate and Springer Nature and as agreed share it, in an anonymised way, for purposes of tracking, analysis and reporting. We will not otherwise disclose your personal data outside the ResearchGate or the Springer Nature group of companies unless we have your permission as detailed in the Privacy Policy.

While Users may use the Springer Nature journal content for small scale, personal non-commercial use, it is important to note that Users may not:

1. use such content for the purpose of providing other users with access on a regular or large scale basis or as a means to circumvent access control;
2. use such content where to do so would be considered a criminal or statutory offence in any jurisdiction, or gives rise to civil liability, or is otherwise unlawful;
3. falsely or misleadingly imply or suggest endorsement, approval , sponsorship, or association unless explicitly agreed to by Springer Nature in writing;
4. use bots or other automated methods to access the content or redirect messages
5. override any security feature or exclusionary protocol; or
6. share the content in order to create substitute for Springer Nature products or services or a systematic database of Springer Nature journal content.

In line with the restriction against commercial use, Springer Nature does not permit the creation of a product or service that creates revenue, royalties, rent or income from our content or its inclusion as part of a paid for service or for other commercial gain. Springer Nature journal content cannot be used for inter-library loans and librarians may not upload Springer Nature journal content on a large scale into their, or any other, institutional repository.

These terms of use are reviewed regularly and may be amended at any time. Springer Nature is not obligated to publish any information or content on this website and may remove it or features or functionality at our sole discretion, at any time with or without notice. Springer Nature may revoke this licence to you at any time and remove access to any copies of the Springer Nature journal content which have been saved.

To the fullest extent permitted by law, Springer Nature makes no warranties, representations or guarantees to Users, either express or implied with respect to the Springer nature journal content and all parties disclaim and waive any implied warranties or warranties imposed by law, including merchantability or fitness for any particular purpose.

Please note that these rights do not automatically extend to content, data or other material published by Springer Nature that may be licensed from third parties.

If you would like to use or distribute our Springer Nature journal content to a wider audience or on a regular basis or in any other manner not expressly permitted by these Terms, please contact Springer Nature at

onlineservice@springernature.com